JACS
JOURNAL OF THE AMERICAN CHEMICAL SOCIETY

Article

pubs.acs.org/JACS

Comparison of DC and AC Transport in 1.5−7.5 nm Oligophenylene Imine Molecular Wires across Two Junction Platforms: Eutectic Ga−In versus Conducting Probe Atomic Force Microscope Junctions

C. S. Suchand Sangeeth,[†,#] Abel T. Demissie,[‡,#] Li Yuan,[†] Tao Wang,[†] C. Daniel Frisbie,[*,‡] and Christian A. Nijhuis[*,†,§]

[†]Department of Chemistry, National University of Singapore, 3 Science Drive 3, Singapore 117543

[‡]Department of Chemical Engineering and Materials Science, University of Minnesota, 421 Washington Avenue SE, Minneapolis, Minnesota 55455, United States

[§]Centre for Advanced 2D Materials and Graphene Research Centre, National University of Singapore, 6 Science Drive 2, Singapore 117546

Supporting Information

ABSTRACT: We have utilized DC and AC transport measurements to measure the resistance and capacitance of thin films of conjugated oligophenyleneimine (OPI) molecules ranging from 1.5 to 7.5 nm in length. These films were synthesized on Au surfaces utilizing the imine condensation chemistry between terephthalaldehyde and 1,4-benzenediamine. Near edge X-ray absorption fine structure (NEXAFS) spectroscopy yielded molecular tilt angles of 33−43°. To probe DC and AC transport, we employed Au−S−OPI//GaO_x/EGaIn junctions having contact areas of 9.6×10^2 μm^2 (10^9 nm^2) and compared to previously reported DC results on the same OPI system obtained using Au−S−OPI//Au conducting probe atomic force microscopy (CP-AFM) junctions with 50 nm^2 areas. We found that intensive observables agreed very well across the two junction platforms. Specifically, the EGaIn-based junctions showed: (i) a crossover from tunneling to hopping transport at molecular lengths near 4 nm; (ii) activated transport for wires >4 nm in length with an activation energy of 0.245 ± 0.008 eV for OPI-7; (iii) exponential dependence of conductance with molecular length with a decay constant β = 2.84 ± 0.18 nm^{-1} (DC) and 2.92 ± 0.13 nm^{-1} (AC) in the tunneling regime, and an apparent β = 1.01 ± 0.08 nm^{-1} (DC) and 0.99 ± 0.11 nm^{-1} (AC) in the hopping regime; (iv) previously unreported dielectric constant of 4.3 ± 0.2 along the OPI wires. However, the absolute resistances of Au−S−OPI//GaO_x/EGaIn junctions were approximately 100 times higher than the corresponding CP-AFM junctions due to differences in metal−molecule contact resistances between the two platforms.

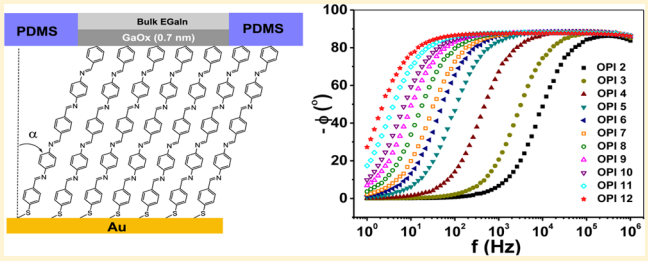

INTRODUCTION

A long-standing goal in molecular electronics is to understand the influence of molecular structure on electrical conduction across metal−molecule−metal junctions.[1−14] Currently, there are a variety of testbeds for measuring electrical transport across molecules such as the break junction,[15,16] the conducting probe atomic force microscope,[17] the scanning tunneling microscope,[18] the eutectic gallium indium alloy (EGaIn) junction,[19−21] the Hg drop junction,[22,23] the conducting polymer junction,[24,25] the surface diffusion mediated junction,[26] and others. However, limited reproducibility of experimental results across different platforms remains a vexing issue that has several possible causes including different types of molecule−electrode contacts (e.g., metal type and chemisorbed vs physisorbed contacts), dissimilar ambient environments (e.g., air vs solvent vs vacuum), and widely varying effective electrical junction areas (i.e., the electrode areas in direct contact with molecules); see Results and Discussion below.[27−29] It is well-known that estimated resistances per molecule can be about 8−9 orders of magnitude smaller in single and few molecule junctions (so-called small area junctions) than junctions consisting of large numbers of molecules (10^3 to 10^{12}) (large area junctions).[28,30] In an excellent review, Akkerman et al. noticed that the estimated resistance per molecule progressively decreases with decreasing junction area, but a good explanation for this general observation across testbeds is lacking.[31] Therefore, a central question in molecular electronics is How reproducible are the electrical characteristics for a given molecular architecture across different types of junctions?[29]

To identify and quantify the factors that cause large discrepancies between testbeds, our goal was to compare transport measurements on well characterized oligophenyleneimine (OPI) wires 1.5−7.5 nm in length using two different junction platforms, namely large area junctions fabricated with the "EGaIn-technique" (EGaIn = eutectic indium gallium alloy,

Received: February 24, 2016
Published: May 12, 2016

DOI: 10.1021/jacs.6b02039
J. Am. Chem. Soc. 2016, 138, 7305−7314

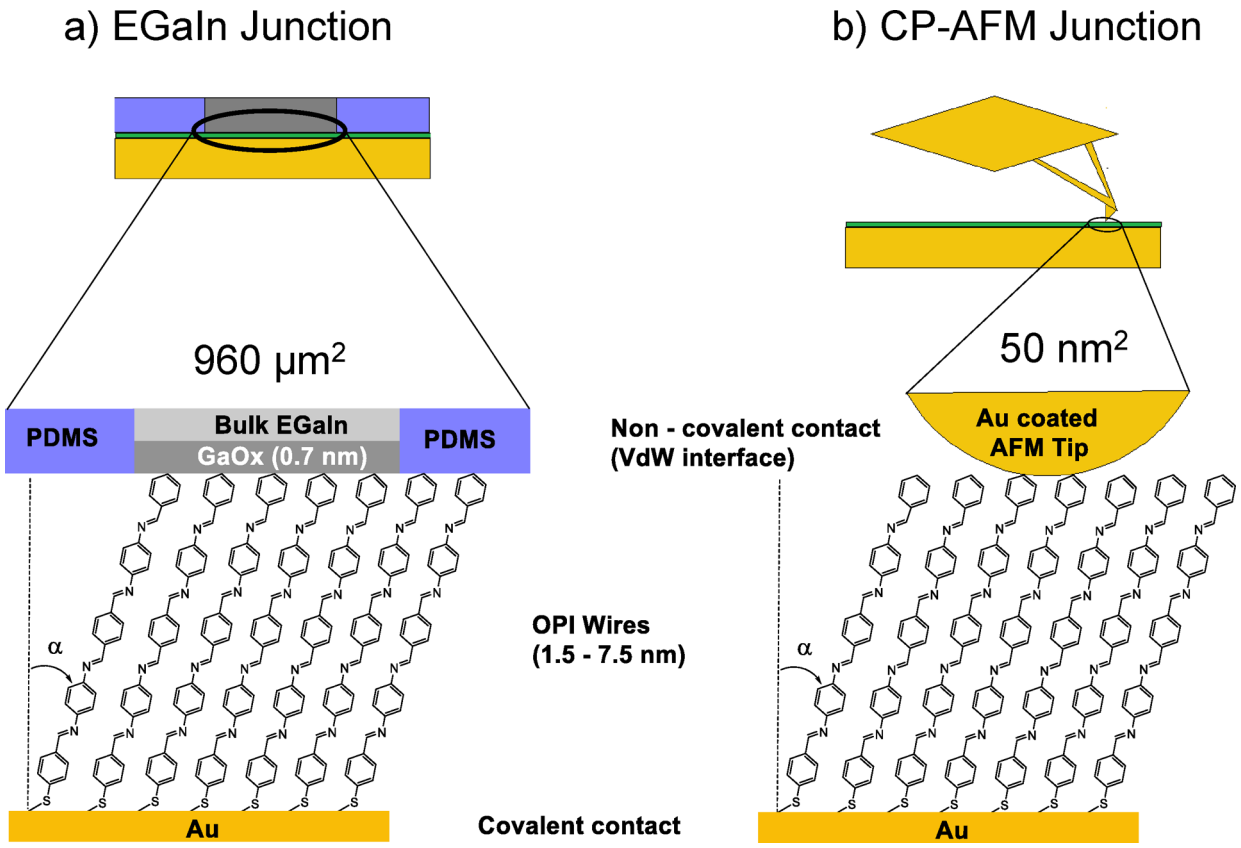

Figure 1. Schematic illustration of the OPI wire based junction. The OPI monolayers are attached to the Au via metal−thiolate bonds and form a van der Waals contact with the top electrode (not drawn to scale). (a) The top-electrode is a non-Newtonian liquid metal stabilized in a through-hole in PDMS. EGaIn = eutectic alloy of Ga and In, GaO_x = native gallium oxide layer which is highly conductive and 0.7 nm thick, PDMS = polydimethylsiloxane.[38,44,69] (b) The top electrode is Au coated AFM tip (∼50 nm in thickness).[36,37,51] Tilt angle α is defined as the angle of the SAM with respect to the surface normal. The illustrations are not drawn to scale.

Figure 1a) and small area junctions fabricated with conducting probe atomic force microscope (CP-AFM, Figure 1b) top electrodes.[32−34] These two platforms have vastly different junction areas of approximately 9.6×10^2 μm^2 and 50 nm^2, respectively, and they also employ different metals (EGaIn/GaO_x vs Au) for the top contact. Thus, these two junctions could be expected to yield very different results for OPI wires. On the contrary, however, we find that certain key measured values described below are identical within error. We note that the OPI system is a good test-case for platform comparison because different charge transport mechanisms are observable in this system. For example, previous CP-AFM results have shown that there is a clear change in transport mechanism from tunneling to thermally assisted hopping as OPI wire length increases.[34−37] The crossover in transport mechanism manifests itself in both the length and temperature dependence of resistance, providing a rich data set for comparison between the two junction testbeds. Initial questions included whether the crossover from tunneling to hopping is observable in large area EGaIn junctions and whether the crossover length and temperature dependence (i.e., activation energy in the hopping regime) were the same as measured by small area CP-AFM based junctions.

In the new EGaIn based data reported here, a clear transition in transport mechanism is indeed observed near 4 nm in wire length, as has been reported previously using CP-AFM.[34−37] That is, for wires <4 nm, the conductance decreases exponentially with length with a decay constant β of 2.92 ± 0.13 nm^{-1}, and for wires >4 nm, the apparent decay constant β is 1.01 ± 0.08 nm^{-1}, similar to the values found by CP-AFM (i.e., 3.0 ± 0.08 and 0.9 ± 0.07 nm^{-1},[37] respectively). Furthermore, for long wires, the transport is thermally activated, consistent with hopping; the activation energy of 0.245 ± 0.008 eV also agrees very well with previous CP-measurements (0.280 eV).[37] From the general molecular electronics perspective, it is gratifying that these two platforms, which differ by 7 orders of magnitude in terms of the contact areas they provide, can achieve such similar results. Furthermore, the EGaIn results reported here represent the first time a clear crossover behavior from tunneling to hopping has been observed in a large area junction, providing confirmation of this important result. However, the resistances of the OPI wires, normalized for effective electrical contact area, differ by 2 orders of magnitude between the two platforms. This is likely due to a combination of imperfect area normalization and differences in contact resistance, a point we will return to later.

Importantly, the EGaIn platform also allows AC impedance measurements on molecular junctions.[38,39] Thus, an additional goal of this work was to perform AC impedance measurements on OPI wires for the first time. These new data corroborate and extend the DC results. Specifically, a simple equivalent circuit consisting of a contact resistance R_C in series with a parallel combination of the OPI resistance (R_{OPI}) and capacitance (C_{OPI}) was sufficient to fit the Nyquist and Bode plots. The R_{OPI} from AC measurements also showed a crossover from

DOI: 10.1021/jacs.6b02039
J. Am. Chem. Soc. 2016, 138, 7305−7314

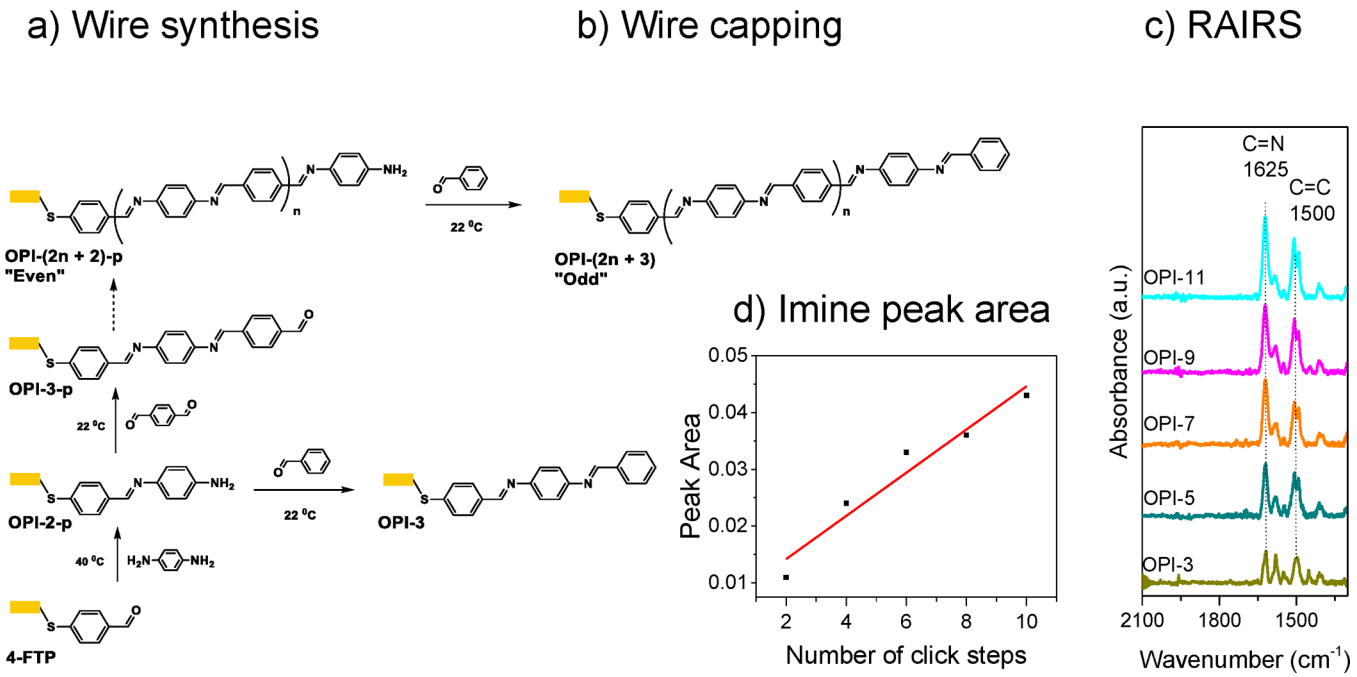

Figure 2. (a) Molecular structure and stepwise wire growth of OPI wires starting from 4-FTP. (b) Molecular structure of OPI wires capped with benzaldehyde, and the corresponding RAIRS spectra (c). (d) Normalized peak area of the C═N (1625 cm^{-1}) stretch mode as a function of the total number of Schiff base reactions.

tunneling to hopping near 4 nm, similar to DC measurements. Furthermore, the dielectric constant of the OPI films normal to the substrate was extracted for the first time from C_{OPI} and the result agreed well with theoretical calculations of conjugated SAMs.[40] In general, the agreement obtained for OPI wires between the EGaIn and CP-AFM testbeds provides a good example of the consistency and reproducibility that can be obtained in current molecular electronics experiments based on well-characterized π-conjugated molecular films.

EXPERIMENTAL METHODS

Materials and Reagents. Au pellets were purchased from Mowrey, Inc. (St. Paul, MN). Silicon wafers were purchased from Wafer Net (San Jose, CA). 4-Aminothiophenol (4-ATP), terephthalaldehyde, 1,4-benzenediamine, and benzaldehyde were purchased from Sigma-Aldrich (St. Louis, MO) and used as received. Absolute ethanol was purchased from Decon Laboratories (King of Prussia, PA), and dimethyl sulfoxide (DMSO) was purchased from Fisher Scientific (Waltham, MA). 4-Formylthiophenol (4-FTP) was synthesized according to the literature.[41,42]

Synthesis of OPI Wires. Au substrates were prepared by electron beam evaporation. Cr (50 Å) was first evaporated on bare Si wafer followed by 500 Å of Au using a CHA evaporator (SEC 600) at a rate of approximately 1 Å/s and base pressure of $\leq 2 \times 10^{-6}$ Torr. The Au substrates were then immersed into purged solutions of 1 mM 4-ATP (absolute ethanol) or 4-FTP (DMSO). After 24 h, the SAM-coated Au substrates were removed from the thiophenol solution and rinsed thoroughly with absolute ethanol to remove physisorbed molecules before immersing them into Ar purged 20 mM solution in ethanol containing the next dialdehyde or diamine derivative depending on the wire design. Detailed synthesis procedures for OPI wires can be found in reference 45.

Surface Characterization (RAIRS, XPS, UPS, and NEXAFS). Reflection−absorption infrared spectra (RAIRS) were collected with a Nicolet iS50 spectrometer with a Harrick Seagull accessory for grazing angle specular reflectance measurements. The incident angle for the *p*-polarized IR beam was 84° from the surface normal. For each sample and background, an average of 300 scans at a resolution of 2 cm^{-1} were collected after 15 min of purging with dry air. The XPS, UPS, and NEXAFS spectroscopy were performed at the SINS (Surface, Interface and Nanostructure Science) beamline at the Singapore Synchrotron Light Source (SSLS).[43] We measured all the samples at room temperature in an ultrahigh vacuum (UHV) chamber with a base pressure of 1×10^{-10} mbar. A sputter-cleaned gold foil was in electrical contact with the samples to calibrate the photon energy of the Au $4f_{7/2}$ core level peak at 84.0 eV. The photon energy resolution was 50 meV. We used a photon energy of 350 eV to probe the C 1s and S 2p states, and of 550 eV to probe the N 1s state. In UPS measurements, we used a photon energy of 60 eV and applied −10 V to the sample to overcome the work function of the analyzer. The UPS spectra were referenced to the Fermi edge of Au (Figure S3). All XPS and UPS spectra were normalized by their photon flux of the synchrotron light recorded during the measurements. We carried out the angular-dependent NEXAFS spectra at C *K*-edge in the Auger electron yield mode with a Scienta R4000 electron energy analyzer. The synchrotron light was linearly *p*-polarized with a polarization degree of 90% and the photon energy resolution was 200 meV. We normalized the NEXAFS spectra to the incident photon flux, and then normalized to have the same absorption edge step height well above the absorption edge. Two incident angles (θ, the angle between the incident light and the sample surface), normal incidence ($\theta = 90°$) and grazing incidence ($\theta = 20°$), were used to record the NEXAFS spectra in order to calculate the tilt angle (α, the angle between the long axis of the molecular wire and the surface normal) of the OPI molecular wire (see detailed methods in Supporting Information page S7).

Junctions with GaO_X/EGaIn Top-Electrodes. The method to form electrical contacts has been reported elsewhere.[44] The GaO_x/EGaIn confined within a through-hole in the transparent rubber PDMS (polydimethylsiloxane) served as the top-electrode with a geometrical area of 9.6×10^2 μm^2. We placed the top-electrode gently in contact with an Au bottom-electrode that supported the OPI wires for conducting the transport measurements. The *J* (V) measurements were carried out using a Keithley 6430 source meter and data were acquired using LabView 2010. We measured the impedance of these junctions using an impedance analyzer (model Solartron 1260A with 1296A dielectric interface) in reference mode with a standard 10 pF capacitor as the external reference. Before we started the impedance measurements, we determined the *J* (V) characteristics of the devices

DOI: 10.1021/jacs.6b02039
J. Am. Chem. Soc. 2016, 138, 7305−7314

and recorded the values of J over the range of biases of −0.50 to 0.50 V (one trace ≡ 0 V → 0.50 V → −0.50 V → 0 V) at intervals of 20 mV. The scan rates for the current voltage measurements were in the range 0.06−0.1 V/s. The temperature dependent J (V) measurements were performed in a probe station (Lakeshore CRX-VF) at a pressure of 3×10^{-5} bar.

RESULTS AND DISCUSSION

Wire Synthesis and Characterization. Figure 2a shows the stepwise growth of OPI wires starting from a monolayer of 4-formylthiophenol (4-FTP); the stepwise growth from a SAM of 4-ATP is shown in the Supporting Information. This method facilitated high yield, subnanometer control of wire length along the sample normal as shown previously.[45] Figure 2b shows the wire capping step, i.e., amine terminated wires with even (4-FTP, Figure 2b) and odd (4-ATP, Figure S1) numbers of phenyl rings were reacted with benzaldehyde to obtain a consistent terminal group which facilitated reproducible electrical characterization. Figure 2c displays the reflection absorption infrared spectroscopy (RAIRS) spectra of capped OPI wires with odd numbers of phenyl units. The intensity of the C═N stretch peak (1625 cm^{-1}) and C═C stretch peak (1500 cm^{-1}) increased with the number of repeat units as expected. Figure 2d represents the normalized peak area of the imine stretch as a function of the total number of click steps, which increases approximately linearly.

Figure 3 shows the angle-dependent NEXAFS spectra of OPI-3, OPI-7, and OPI-11, and the tilt angles (α; defined in Figure 1) of the molecular wires (spectra of OPI-5, and OPI-9 are plotted in Figure S2). The values of α for all five molecules we measured are between 33° and 43°, which is in line with other reported values of α for SAMs of molecular wire systems on Au surfaces with a standing-up phase.[46] Thus, the NEXAFS data reveal that the OPI molecular wires from n = 3 to 11, i.e., from short to long wire regimes, are tilted.

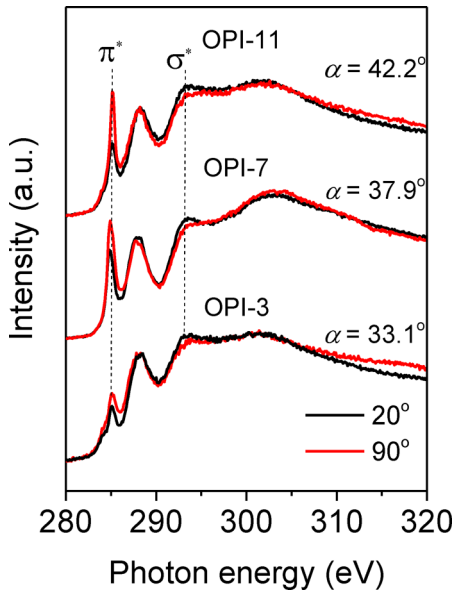

Figure 3. Angle dependent C K-edge NEXAFS spectra of OPI-3, OPI-7, and OPI-11. The black and red traces correspond to 20° and 90° incident angles, respectively, measured from the sample surface.

DC Characteristics. Figure 4a displays the $J(V)$ characteristics of OPI wires measured with the EGaIn technique. The $J(V)$ data are often interpreted using the general tunneling equation (eq 1) where β is the decay constant, d is the length of the OPI wire (in nm), and $J_0(V)$ is the hypothetical current through the junction for d = 0 nm.

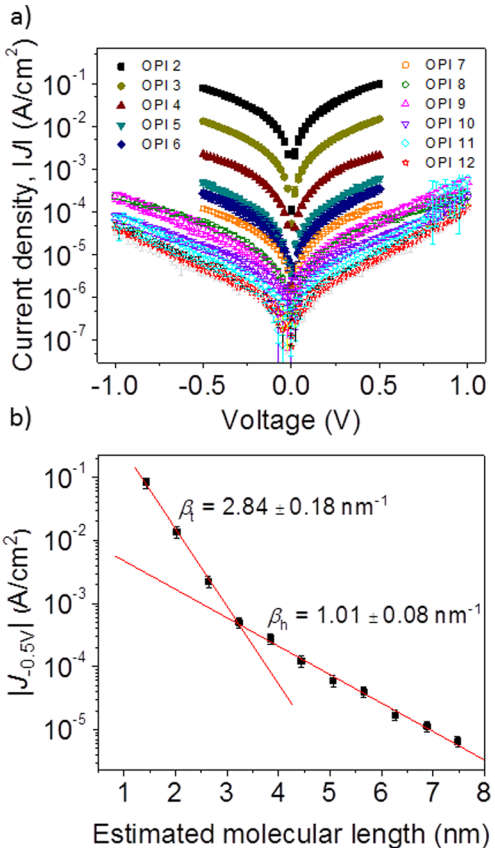

Figure 4. DC J−V measurements on EGaIn junctions. (a) The average $J(V)$ traces for the Au-OPI//GaO_x/EGaIn junctions for OPI wires of different lengths. (b) J vs molecular length at V = −0.5 V. The red solid line represents fit to eq 1. Error bars represent 3 standard deviations.

$$J(V) = J_0(V)e^{-\beta d} \quad (1)$$

Equation 1 implies that at a given bias, the current density (J) decreases with increasing d. Figure 4b shows the semilog plot of J at V = −0.5 V versus d revealing two distinct regimes of the exponential decay of J with a crossover near 4 nm. The error bars represent 1 standard deviations derived from a total of 60 scans recorded at 3 different sample locations. The change in the value of β indicates that the transport mechanisms in the short and long molecular wires are different. The red solid lines represent fits to eq 1. The short molecular wires (OPI 2−OPI 5) yield β = 2.84 ± 0.18 nm^{-1}, while the long molecular wires yield an apparent β = 1.01 ± 0.08 nm^{-1} ("apparent" because tunneling does not occur in this regime; see below). The absence of hysteresis in the $J(V)$ curves obtained from both platforms indicates that charging effects can be neglected. We wish to note that the role of defects in the EGaIn junctions have been studied in detail and can be neglected provided ultraflat bottom-electrodes are used and the geometrical junction area is kept below 9.6×10^2 μm^2.[47,48]

The value of β depends on various factors including the nature of the bonds in the molecular backbone, energy level alignment, and transport mechanism.[49,50] The β value of 2.84 ± 0.18 nm^{-1} is typically observed for aromatic monolayers in the

DOI: 10.1021/jacs.6b02039
J. Am. Chem. Soc. 2016, 138, 7305−7314

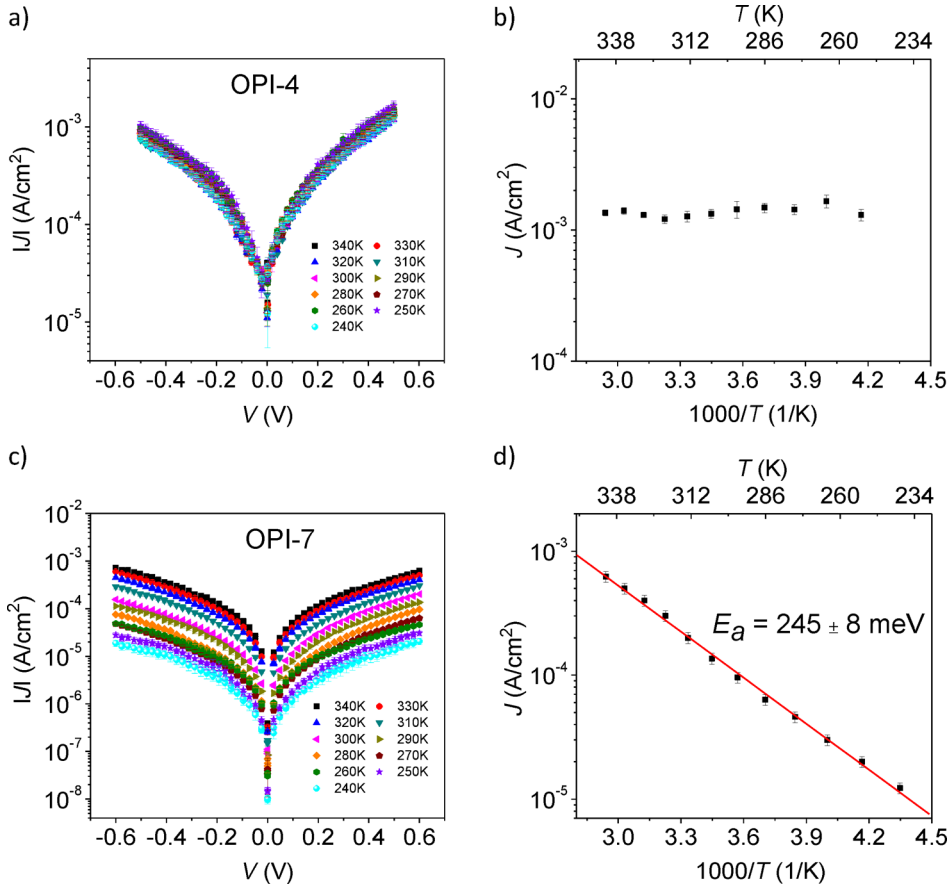

Figure 5. Variable temperature EGaIn DC bias measurements for (a) OPI-4 and (c) OPI-7 wires. The activation energy was calculated from the Arrhenius plot of ln $J(T)$ versus $(1/T)$. Error bars represent one standard deviation.

tunneling regime, but the very low value of β = 1.01 ± 0.08 nm^{-1} is characteristic for hopping (note that here we did not change the nature of the backbone of the SAM or the nature of the molecule-electrode interfaces). In hopping transport, charge is injected into the molecular backbone from one contact, and driven along to the other contact via the applied electric field. This regime has different temperature, bias, and length dependences than the tunneling regime.[36,37,51−55] Lateral or intermolecular charge transport can be neglected since the electric field is very large along the sample normal (approximately 2 MV/cm). Nevertheless, it is very clear that there is a change in the length dependence when wire length crosses over 3−4 nm.

To confirm the mechanism crossover, we performed temperature dependent $J(V)$ measurements on short (OPI 4) and long (OPI 7) molecular wires. The $J(V,T)$ data are shown in Figure 5. Junctions with the short molecular wire OPI 4 show temperature independent $J(V)$ curves indicating that charge transport in these short wires is dominated by through bond tunneling. On the other hand, the temperature dependent $J(V)$ curves for junctions with OPI 7 indicate that the long molecular wires display activated hopping transport. We determined the activation energy, E_a, by fitting the plot of ln J versus $1/T$ at V = 0.6 V (Figure 5d) to the Arrhenius equation (eq 2):

$$J(V, T) = J_0(V) \exp\left(\frac{-E_a}{k_B T}\right) \quad (2)$$

where k_B is the Boltzmann constant. For junctions with OPI 7 wires, we found E_a = 245 ± 8 meV.

The origin of the activation energy, E_a, may be rationalized on the basis of the Marcus theory of electron transfer, which is expressed by eq 3:[56,57]

$$k_{ET} = \sqrt{\frac{\pi}{\hbar^2 k_B T \lambda}} H^2 \exp\left(-\frac{(\lambda + \Delta G^\circ)^2}{4\lambda k_B T}\right) \quad (3)$$

where k_{ET} is the charge hopping rate, H is the effective Hamiltonian that couples initial and final states, ΔG° is the voltage-dependent thermodynamic driving force, λ is the reorganization energy and includes contributions from electronic and nuclear rearrangements, and T is the temperature. Thus, E_a can be expressed as $(\lambda_{total} + \Delta G^\circ)^2/4\lambda_{total}$. The obtained value of 245 ± 8 meV for E_a is comparable to our previous result for OPI wires by CP-AFM,[37] and decreases with applied bias as shown in Figure S5. This decrease is likely due to the increase in $|\Delta G^\circ|$ with applied V. Our previous work on oligonapthalenefluoroeneimine (ONI) wires[34] and oligo-tetrathiafulvalene-pyromelliticdiimide-imine (OTPI) wires[35] has shown that E_a is influenced by molecular conformation (e.g., planarity), and the HOMO−LUMO gap (extent of delocalization). For OPI wires, the ultraviolet (UV) visible absorption spectra indicate that conjugation does not extend over the entire wire, i.e., the optical band gap does not reduce beyond OPI-3,[37] consistent with the picture that the charge makes multiple hops along each chain. E_a may depend on torsional motions within the OPI wires that transiently couple

DOI: 10.1021/jacs.6b02039
J. Am. Chem. Soc. 2016, 138, 7305−7314

conjugated subunits along the chain.[51] Indeed 245 meV corresponds very well to the typical torsional vibrations in conjugated molecules. If ΔG° is estimated to be around −25 meV (for low bias), then the solution to $E_a = (\lambda_{total} + \Delta G^\circ)^2/4\lambda_{total}$ yields total reorganization energy of ∼1.1 eV. Detailed analysis of E_a is, however, not our principal focus here.

AC Characteristics. An important advantage of the EGaIn molecular junction versus other platforms is that it can be employed easily to measure AC transport by impedance spectroscopy.[38,39,58] The complex impedance Z is more general than resistance since it contains amplitude and phase information.[59] Figure 6a shows the frequency dependence of

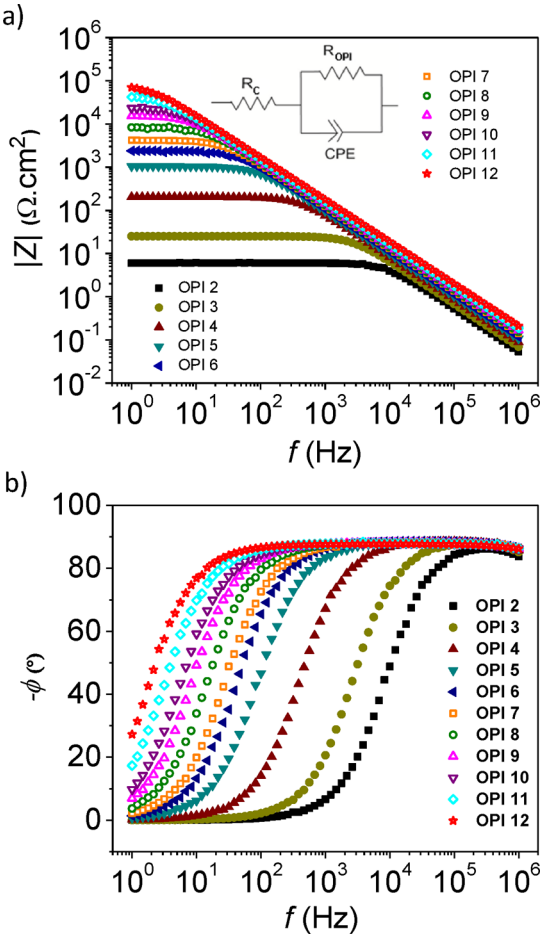

Figure 6. EGaIn AC Impedance measurements. (a) Frequency dependence of |Z| for different OPI wire length. (b) The phase angle vs frequency plots.

the modulus of the complex impedance (|Z|) for different molecular wires (OPI-2 to OPI-12) formed on Au. The Nyquist plots (Figure S6) show only one semicircle which indicates the presence of one capacitor (C_{OPI}) in the equivalent circuit. The modulus |Z| increases over 4 orders of magnitude as the estimated molecular length changes from 1.5 nm (OPI 2) to 7.5 nm (OPI 12). The frequency dependence of |Z| is nearly constant at low frequencies (dominated by the resistance of the molecular wire), but decreases with increasing frequency as the capacitive reactance ($X_c = 1/\omega^n C_{OPI}$) decreases with frequency ω.[38,39]

To fit the impedance data, we used an equivalent circuit consisting of a contact resistance R_C in series with a parallel combination of a constant phase element (CPE) and R_{OPI}. The CPE is modeled by an additional exponential empirical constant (n) on the reactance equation that is often used to account for nonideal capacitance due to defects in the semiconductor material (e.g., grain boundaries and surface roughness). For $n = 1$, the CPE is the same as an ideal capacitor. Table S1 shows that $n = 0.99-0.994$ for the short wires but then monotonically decreases to 0.975 for the long wires. In this study, we used e-beam deposited Au films that generate relatively small grains with deep grain boundaries, compared with smooth surfaces, i.e., template-stripped Au substrates (more later). Thus, there are defects in the wires caused by the topography of the Au films resulting in n values slightly lower than 1. The small decrease in the value of n as a function of wire length is likely caused by a small increase in the number of defects with wire length. Importantly, the plateau value at low frequency in Figure 6a is equal to the sum of R_C and R_{OPI}.

Figure 6b shows the phase ϕ against the frequency. The phase increases to 90° as the frequency increases, and high frequency impedance is dominated by the capacitance (for capacitors, ϕ is 90°, while for ideal resistors, ϕ is 0°). From Figure 6a,b, it is therefore clear that up to a roll-off frequency associated with the kinks in the |Z| vs ω and the ϕ vs ω curves, the wires exhibit resistive behavior. For frequencies higher than the roll-off ω, the response becomes increasingly capacitive. We were able to fit the Figure 6a behavior to eq 4 based on the equivalent circuit described above.

$$Z = R_C + \frac{R_{OPI}}{1 + R_{OPI}^2\omega^{2n}C_{OPI}^2} - j\left(\frac{\omega^n C_{OPI}R_{OPI}^2}{1 + R_{OPI}^2\omega^{2n}C_{OPI}^2}\right) \quad (4)$$

The values of R_{OPI}, C_{OPI}, and n for each wire obtained from the fit are summarized in Table S1.

Figure 7a displays the molecular length dependence of R_{OPI} obtained by impedance measurements. Clearly short OPI wires show a different trend compared to the long molecular wires. Near a molecular length of 4 nm, the OPI wires show a transition in the slope. Modifying eq 1, we can relate d to R_{OPI} where $R_{OPI,0}$ is the pre-exponential factor.

$$R_{OPI} = R_{OPI,0}e^{\beta d} \quad (5)$$

When we fit the data in Figure 7a to eq 5, the short molecular wires (OPI 2−OPI 5) yield $\beta = 2.92 \pm 0.13$ nm^{-1}, while the long molecular wires yield an apparent $\beta = 0.99 \pm 0.11$ nm^{-1}. These β values are close to the values estimated using the DC $J(V)$ data (Figure 5) indicating the consistency in our transport measurements. Figure 7b shows the variation of contact resistance with molecular length. The contact resistance is likely dominated by the molecular wire//GaO_x interface which is of van der Waals type. The molecular length independent R_C indicates that the van der Waals type interface is similar for all the molecules as observed for other molecular systems with GaO_x/EGaIn as top contact.[38,39]

C_{OPI} is plotted as a function of $1/d$ in Figure 7c and it follows a straight line fit given by the parallel plate capacitance relation (eq 6)

$$C_{OPI} = \varepsilon_0\varepsilon_{r,OPI}A_{geo}/d \quad (6)$$

where ε_0 is the permittivity of the free space, $\varepsilon_{r,OPI}$ is the dielectric constant of the wires, and A_{geo} is the geometrical area of the electrode. Fitting C_{OPI} values to eq 6 gave a value of $\varepsilon_{r,OPI}$

DOI: 10.1021/jacs.6b02039
J. Am. Chem. Soc. 2016, 138, 7305−7314

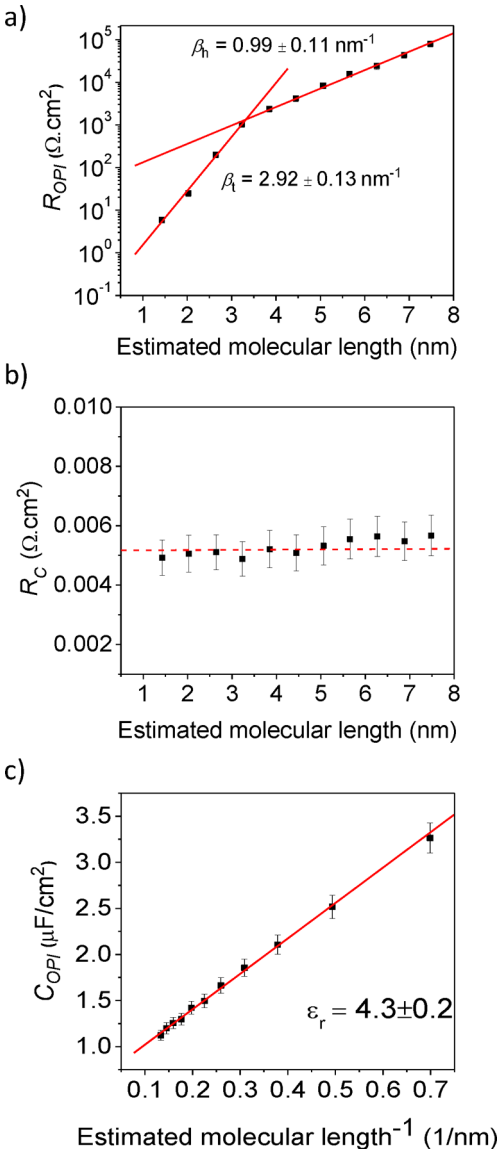

Figure 7. EGaIn AC impedance results. (a) Resistance of the molecular wires (R_{OPI}) vs length. Red solid lines are fits to eq 5. (b) The contact resistance (R_C) as a function of wire length. The red dashed line is a guide to the eye. (c) Capacitance of the molecular wires (C_{OPI}) vs inverse length. The red solid line represents the fit to parallel plate capacitance relation (eq 6). Error bars represent 3 standard deviations.

of 4.3 ± 0.2. This parallel capacitance model holds for our system because the separation between the plates (length of OPI films) is much smaller than the contact area. The error bars were tabulated using the nonlinear least-square method from a total of 15 scans at 3 different sample locations.

Recently, Ratner et al. used first principle calculations to show that the dielectric constant is strongly influenced by the SAM properties such as polarizability, surface coverage, tilt angle, and configuration.[40] Our obtained $\varepsilon_{r,OPI}$ value of 4.3 is approximately 17−20% different than the calculated ε_r values of conjugated polyyne SAMs. Even though our OPI wires contain more polarizable repeat units than polyyne SAMs, the nonzero dihedral and tilt angles of the OPI wires disrupt molecular planarity and suppress electron cloud polarizability by the electric field, which presumably results in lower $\varepsilon_{r,OPI}$ values.

Comparison of EGaIn and CP-AFM Measurements. When comparing molecular electronics testbeds, it is important to identify quantities that are intensive, i.e., independent of the junction area, versus extensive, i.e., dependent on junction area. Considerable uncertainties in junction areas can make comparison of extensive quantities difficult. However, intensive quantities should be directly comparable.

Measured Intensive Quantities. The area independent transport characteristics such as β, crossover length, hopping decay slope, and E_a are summarized in Table 1 for both CP-AFM and EGaIn junctions. There is remarkable agreement between the intensive transport characteristics of EGaIn and CP-AFM junctions. The β values for instance agree within 10%, the crossover lengths are identical, and the activation energies agree within 13%. Collectively, these results indicate exceptional reproducibility in these key area-independent transport parameters across two very different platforms for charge transport.

Table 1. Comparison of Intensive (Area Independent) Transport Characteristics of CP-AFM and EGaIn Junctions

junction platform	$\beta_{Tunneling}$ (nm^{-1})	crossover length (nm)	activation energy (meV)	$\beta_{Hopping}$ (nm^{-1})
CP-AFM[37]	3.0 ± 0.08	4	280	0.9 ± 0.07
DC EGaIn	2.84 ± 0.18	4	245 ± 8	1.01 ± 0.08
AC EGaIn	2.92 ± 0.13	4	NA	0.99 ± 0.11

Measured Extensive Quantities. On the other hand, it is far more challenging to compare absolute resistance values for the two junctions as resistance depends on the number of molecules in active electrical contact. Further, the geometrical contact areas for the EGaIn and CP-AFM junctions differ by a factor of ~10^7. Computational work by Landau et al. has shown that for junctions with tens of molecules, the conductance should scale linearly with the number of contacted molecules.[60] Thus, the total resistance can be described by eq 7:

$$1/R_{OPI} = 1/r + 1/r + 1/r... = n_{mol}/r = \Gamma_{OPI}A/r \quad (7)$$

where r is the resistance per molecule, and n_{mol} is the number of molecules in the junction, which is determined by the surface coverage (Γ_{OPI}) and junction area (A). The surface coverage for OPI wires on Au was found previously to be 3.5 molecules/nm^2.[45] Note that this coverage value is the same for both the EGaIn and CP-AFM platforms as both used OPI wires grown on Au prepared by the same method. With the use of this coverage value, the total number of molecules within the CP-AFM junction is approximately 200, and 3 × 10^9 for the EGaIn junction based on the geometrical contact areas.

Figure 8 displays the estimated single molecule resistances r as a function of d for CP-AFM junctions along with the measured AC and DC r values for the EGaIn junctions. The initial values (black squares vs blue triangles) differ by a colossal 6−7 orders of magnitude. The relevant sources of discrepancies between the two testbeds are discussed below.

Correcting for the Effective EGaIn Electrode Contact Area. Akkerman et al. summarized in a review that the observed resistance per molecule increases with increasing geometrical area of the junctions.[28] In other words, the observed resistances per molecule in large area SAM based junctions are 7 orders of magnitude larger than those values obtained from single molecule experiments.[28] Whitesides et al. postulated that one of the "culprits" for this large discrepancy could be the difference

DOI: 10.1021/jacs.6b02039
J. Am. Chem. Soc. 2016, 138, 7305−7314

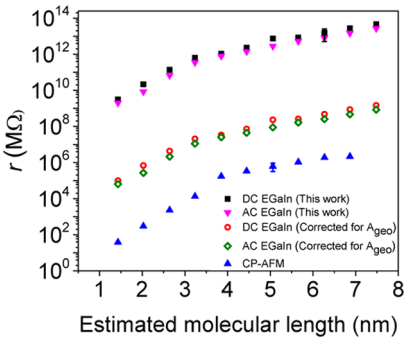

Figure 8. A semilog plot of resistance per molecule versus molecular length for OPI wires obtained from CP-AFM[37] and EGaIn testbeds. Representative error bars are shown on select points.

between effective electrical contact area (area of the electrode in direct contact with molecules) and the geometrical contact area.[61,62] Their results showed that the effective contact area of the EGaIn top contact is approximately 10^{-4} times smaller than the geometrical contact area for alkyl thiol SAMs on a template-stripped Ag substrate.[61] In that work, a correction factor of 10^{-3} was reported to account for the surface roughness of the EGaIn/GaO_x top-contact and an additional roughness factor of 10^{-1} was included for the template stripped bottom-contact.

Correcting for the Au Substrate Roughness. In this study, the relatively large roughness associated with thermally deposited Au (not template-stripped) further reduces the total number of contacted molecules. The correction factor for the bottom Au electrode was calculated using a similar method outlined by Whitesides et al. based on a high resolution STM image of the Au electrode.[61] The STM image pixel count within the first 2 Å from the topmost average plane of the image in Figure 9 was calculated, and this resulted in an additional roughness correction factor of $10^{-1.5}$. This correction, combined with the factor of 10^{-3} mentioned above for the EGaIn electrode, gives a combined area correction factor of $10^{-4.5}$. The red and green data points in Figure 8 show the r vs d behavior after correcting by this factor. It is clear that there is still a large difference between the EGaIn and CP-AFM values of r of approximately a factor of 10^2.

Role of Contact Resistance and Electrode Work Function. Importantly, based on the red and blue data points in Figure 8, we estimate that the contact resistances *per molecule* for DC EGaIn and CP-AFM junctions are approximately 500 and 1 MΩ, respectively, a substantial difference. These contact resistances (at d = 0 nm) were extrapolated from linear fits of the semilog plots of r vs d in the tunneling regimes (red and blue symbols in Figure 8). It is well-known that contact resistances are strongly influenced by the work function of the electrodes and nature of contact (physisorbed vs chemisorbed).[49,63−67] For example, we have previously reported that contact resistance for SAMs of alkyl thiols decreased by 2 orders of magnitude with increasing work function of the metal contacts.[64] That is, contact effects can result in orders of magnitude changes in absolute resistance; the effects are comparable to the corrections for effective contact area. It is not surprising that the contact resistance is substantially higher for EGaIn versus CP-AFM junctions given the presence of the GaO_x interlayer and the lower work function of EGaIn versus Au top contact (4.2 vs 5.1 eV). In EGaIn junctions, the native 0.7 nm thick layer of GaO_x acts as a protective barrier that prevents the bulk EGaIn from alloying with the bottom-

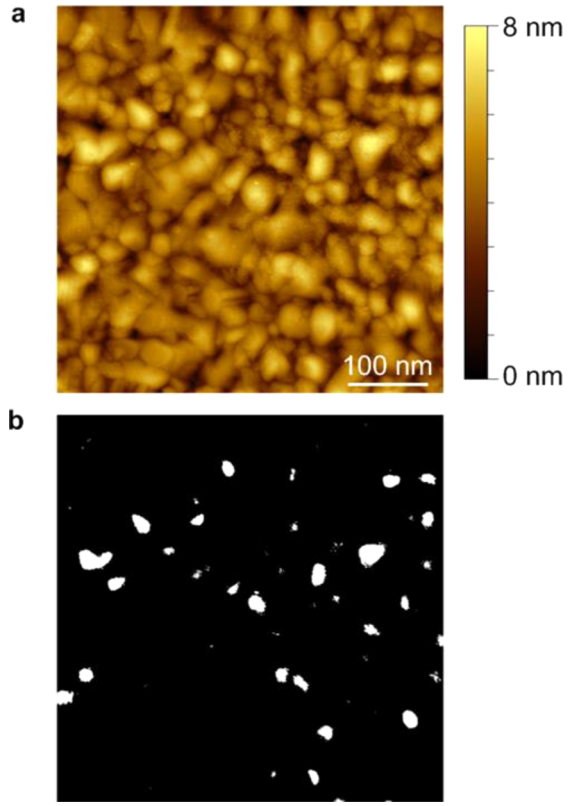

Figure 9. (a) Scanning tunneling microscopy image of a typical Au substrate. (b) Surface area available for contact (white area) estimated via digital analysis of the STM image in (a). The contact area (3.1%) was estimated as the number of pixels within 2 Å from the topmost average plane of the image in (a).

electrode. It has been shown that resistance of GaO_x is about 100 times more than that of bulk EGaIn.[17,38,39,61] For these reasons, we believe that the difference in the observed values of r between the CP-AFM and EGaIn junctions of 2 orders of magnitude (after correction for effective electrical contact area) is caused by contact resistance between the SAM//top-electrode.

■ CONCLUSION

DC and AC electrical characterization have been measured for a set of systematically synthesized conjugated oligophenyleneimine wires varying between 1.5 and 7.5 nm in molecular length via the EGaIn top contact approach. The EGaIn junction affords access to both AC measurements and high precision variable temperature measurements which are critical for understanding transport mechanisms. The DC bias J−V results indicated a clear crossover from tunneling to hopping transport near 4 nm. Thus, this crossover was confirmed in a large area junction previously observed only in CP-AFM based junctions. Variable temperature measurements indicated thermally activated transport for long wires with activation energy of 0.245 ± 0.008 eV in line with previously reported CP-AFM data. AC impedance spectroscopy measurements were utilized to calculate the wire resistance, wire capacitance, and for the first time, the dielectric constant of the wires. The AC results also indicated a similar crossover from tunneling to hopping transport near 4 nm with a decay constant β of 2.92 ± 0.13 nm^{-1} in the tunneling regime, and 0.99 ± 0.11 nm^{-1} in the hopping regime. Our results show excellent overall agreement

DOI: 10.1021/jacs.6b02039
J. Am. Chem. Soc. 2016, 138, 7305−7314

between EGaIn and CP-AFM junctions for the measured intensive (area independent) quantities such as the length decay constant, crossover length, and activation energy. On the basis of these results, we conclude the differences in estimated resistance per molecule (extensive, area dependent quantity) in our large and small area junctions reflect correction factors for effective contact area due to roughness and contact resistance due to differences in the work function of the electrodes. Future work will exploit the impedance spectroscopy and variable temperature approaches afforded by the EGaIn junctions to examine the connection between wire architecture and transport in the hopping regime.

Studies that compare charge transport characteristics for a given molecular structure to gauge reproducibility across different testbeds are rare, though there are prior examples. For example, Chiechi et al. found good agreement between EGaIn and CP-AFM junctions based on monolayers of photosystem I.[68] However, due to the lack of cross testbed studies, a general explanation for the large observed discrepancy in absolute resistances per molecule is lacking.[29] In agreement with Whitesides et al.,[61] our results indicate that the surface roughness of the electrodes can account for 5 orders of magnitude of spread in the data. We believe in our case that the molecule—electrode contact resistances account for 2 orders of magnitude difference in absolute values of r. More studies are needed to confirm whether effective contact areas and contact resistances can in general account for the large spread of r values across other small and large area junctions.

■ ASSOCIATED CONTENT

Supporting Information

The Supporting Information is available free of charge on the ACS Publications website at DOI: 10.1021/jacs.6b02039.

Additional experimental details, STM images, Nyquist plots (PDF)

■ AUTHOR INFORMATION

Corresponding Authors

*frisbie@umn.edu

*chmnca@nus.edu.sg

Author Contributions

#C.S.S.S. and A.T.D. contributed equally to this work.

Notes

The authors declare no competing financial interest.

■ ACKNOWLEDGMENTS

The Singapore National Research Foundation (NRF Award No.NRF-RF 2010-03 to C.A.N.) is gratefully acknowledged for supporting this research. This project was also funded by the United States National Science Foundation under Award CHE-1213876, and by the University of Minnesota Industrial Partnership for Research in Interfacial Materials & Engineering (IPRIME). Parts of this work were carried out in the Characterization Facility, University of Minnesota, which receives partial support from NSF through the MRSEC program (DMR-1420013).

■ REFERENCES

(1) Perrin, M. L.; Verzijl, C. J. O.; Martin, C. A.; Shaikh, A. J.; Eelkema, R.; van Esch, J. H.; van Ruitenbeek, J. M.; Thijssen, J. M.; van der Zant, H. S. J.; Dulić, D. *Nat. Nanotechnol.* **2013**, *8*, 282.

(2) Wang, L.; Rangger, G. M.; Romaner, L.; Heimel, G.; Bucì ko, T.; Ma, Z.; Li, Q.; Shuai, Z.; Zojer, E. *Adv. Funct. Mater.* **2009**, *19*, 3766.

(3) Bâldea, I.; Xie, Z.; Frisbie, C. D. *Nanoscale* **2015**, *7*, 10465.

(4) Heimel, G.; Brédas, J.-L. *Nat. Nanotechnol.* **2013**, *8*, 230.

(5) Capozzi, B.; Xia, J.; Adak, O.; Dell, E. J.; Liu, Z.-F.; Taylor, J. C.; Neaton, J. B.; Campos, L. M.; Venkataraman, L. *Nat. Nanotechnol.* **2015**, *10*, 522.

(6) Heimel, G.; Rissner, F.; Zojer, E. *Adv. Mater.* **2010**, *22*, 2494.

(7) Egger, D. A.; Rissner, F.; Zojer, E.; Heimel, G. *Adv. Mater.* **2012**, *24*, 4403.

(8) Abu-Husein, T.; Schuster, S.; Egger, D. A.; Kind, M.; Santowski, T.; Wiesner, A.; Chiechi, R.; Zojer, E.; Terfort, A.; Zharnikov, M. *Adv. Funct. Mater.* **2015**, *25*, 3943.

(9) Toledano, T.; Sazan, H.; Mukhopadhyay, S.; Alon, H.; Lerman, K.; Bendikov, T.; Major, D. T.; Sukenik, C. N.; Vilan, A.; Cahen, D. *Langmuir* **2014**, *30*, 13596.

(10) Fereiro, J. A.; Kondratenko, M.; Bergren, A. J.; McCreery, R. L. *J. Am. Chem. Soc.* **2015**, *137*, 1296.

(11) Motiei, L.; Lahav, M.; Gulino, A.; Iron, M. A.; van der Boom, M. E. *J. Phys. Chem. B* **2010**, *114*, 14283.

(12) Sikes, H. D.; Smalley, J. F.; Dudek, S. P.; Cook, A. R.; Newton, M. D.; Chidsey, C. E.; Feldberg, S. W. *Science* **2001**, *291*, 1519.

(13) Tuccitto, N.; Ferri, V.; Cavazzini, M.; Quici, S.; Zhavnerko, G.; Licciardello, A.; Rampi, M. A. *Nat. Mater.* **2009**, *8*, 41.

(14) Sakamoto, R.; Wu, K.-H.; Matsuoka, R.; Maeda, H.; Nishihara, H. *Chem. Soc. Rev.* **2015**, *44*, 7698.

(15) Perrin, M. L.; Frisenda, R.; Koole, M.; Seldenthuis, J. S.; Gil, J. A. C.; Valkenier, H.; Hummelen, J. C.; Renaud, N.; Grozema, F. C.; Thijssen, J. M.; Dulić, D.; van der Zant, H. S. J. *Nat. Nanotechnol.* **2014**, *9*, 830.

(16) Hines, T.; Diez-Perez, I.; Hihath, J.; Liu, H.; Wang, Z. S.; Zhao, J.; Zhou, G.; Müllen, K.; Tao, N. *J. Am. Chem. Soc.* **2010**, *132*, 11658.

(17) Wold, D. J.; Frisbie, C. D. *J. Am. Chem. Soc.* **2000**, *122*, 2970.

(18) Lauhon, L. J.; Ho, W. *Phys. Rev. Lett.* **2000**, *85*, 4566.

(19) Nijhuis, C. A.; Reus, W. F.; Whitesides, G. M. *J. Am. Chem. Soc.* **2009**, *131*, 17814.

(20) Nijhuis, C. A.; Reus, W. F.; Barber, J. R.; Whitesides, G. M. *J. Phys. Chem. C* **2012**, *116*, 14139.

(21) Chiechi, R. C.; Weiss, E. A.; Dickey, M. D.; Whitesides, G. M. *Angew. Chem., Int. Ed.* **2008**, *47*, 142.

(22) Yaffe, O.; Ely, T.; Har-Lavan, R.; Egger, D. A.; Johnston, S.; Cohen, H.; Kronik, L.; Vilan, A.; Cahen, D. *J. Phys. Chem. C* **2013**, *117*, 22351.

(23) Tran, E.; Rampi, M. A.; Whitesides, G. M. *Angew. Chem., Int. Ed.* **2004**, *43*, 3835.

(24) Akkerman, H. B.; Blom, P. W. M.; de Leeuw, D. M.; de Boer, B. *Nature* **2006**, *441*, 69.

(25) Neuhausen, A. B.; Hosseini, A.; Sulpizio, J. A.; Chidsey, C. E. D.; Goldhaber-Gordon, D. *ACS Nano* **2012**, *6*, 9920.

(26) Bonifas, A. P.; McCreery, R. L. *Nat. Nanotechnol.* **2010**, *5*, 612.

(27) Salomon, A.; Cahen, D.; Lindsay, S.; Tomfohr, J.; Engelkes, V. B.; Frisbie, C. D. *Adv. Mater.* **2003**, *15*, 1881.

(28) Akkerman, H. B.; de Boer, B. *J. Phys.: Condens. Matter* **2008**, *20*, 013001.

(29) McCreery, R. L.; Bergren, A. J. *Adv. Mater.* **2009**, *21*, 4303.

(30) Milani, F.; Grave, C.; Ferri, V.; Samorì, P.; Rampi, M. A. *ChemPhysChem* **2007**, *8*, 515.

(31) Bergren, A. J.; Harris, K. D.; Deng, F.; McCreery, R. L. *J. Phys.: Condens. Matter* **2008**, *20*, 374117.

(32) Wold, D. J.; Frisbie, C. D. *J. Am. Chem. Soc.* **2001**, *123*, 5549.

(33) Engelkes, V. B.; Beebe, J. M.; Frisbie, C. D. *J. Phys. Chem. B* **2005**, *109*, 16801.

(34) Choi, S. H.; Risko, C.; Delgado, M. C. R.; Kim, B.; Brédas, J.-L.; Frisbie, C. D. *J. Am. Chem. Soc.* **2010**, *132*, 4358.

(35) Choi, S. H.; Frisbie, C. D. *J. Am. Chem. Soc.* **2010**, *132*, 16191.

(36) Luo, L.; Balhorn, L.; Vlaisavljevich, B.; Ma, D.; Gagliardi, L.; Frisbie, C. D. *J. Phys. Chem. C* **2014**, *118*, 26485.

(37) Choi, S. H.; Kim, B.; Frisbie, C. D. *Science* **2008**, *320*, 1482.

DOI: 10.1021/jacs.6b02039
J. Am. Chem. Soc. 2016, 138, 7305−7314

(38) Sangeeth, C. S. S.; Wan, A.; Nijhuis, C. a. *J. Am. Chem. Soc.* **2014**, *136*, 11134.
(39) Sangeeth, C. S.; Wan, A.; Nijhuis, C. A. *Nanoscale* **2015**, *7*, 12061.
(40) Heitzer, H. M.; Marks, T. J.; Ratner, M. A. *ACS Nano* **2014**, *8*, 12587.
(41) Golchoubian, H.; Hosseinpoor, F. *Molecules* **2007**, *12*, 304.
(42) Norman Young, R.; Yves Gauthier, J.; Coombs, W. *Tetrahedron Lett.* **1984**, *25*, 1753.
(43) Yu, X.; Wilhelmi, O.; Moser, H. O.; Vidyaraj, S. V.; Gao, X.; Wee, A. T. S.; Nyunt, T.; Qian, H.; Zheng, H. *J. Electron Spectrosc. Relat. Phenom.* **2005**, *144−147*, 1031.
(44) Wan, A.; Jiang, L.; Sangeeth, C. S. S.; Nijhuis, C. A. *Adv. Funct. Mater.* **2014**, *24*, 4442.
(45) Demissie, A. T.; Haugstad, G.; Frisbie, C. D. *J. Am. Chem. Soc.* **2015**, *137*, 8819.
(46) Love, J. C.; Estroff, L. A.; Kriebel, J. K.; Nuzzo, R. G.; Whitesides, G. M. *Chem. Rev.* **2005**, *105*, 1103.
(47) Yuan, L.; Jiang, L.; Zhang, B.; Nijhuis, C. A. *Angew. Chem., Int. Ed.* **2014**, *53*, 3377.
(48) Jiang, L.; Sangeeth, C. S. S.; Wan, A.; Vilan, A.; Nijhuis, C. A. *J. Phys. Chem. C* **2015**, *119*, 960.
(49) Kim, B.; Choi, S. H.; Zhu, X.-Y.; Frisbie, C. D. *J. Am. Chem. Soc.* **2011**, *133*, 19864.
(50) Beebe, J. M.; Engelkes, V. B.; Liu, J.; Gooding, J. J.; Eggers, P. K.; Jun, Y.; Zhu, X.; Paddon-Row, M. N.; Frisbie, C. D. *J. Phys. Chem. B* **2005**, *109*, 5207.
(51) Smith, C. E.; Odoh, S. O.; Ghosh, S.; Gagliardi, L.; Cramer, C. J.; Frisbie, C. D. *J. Am. Chem. Soc.* **2015**, *137*, 15732.
(52) Goldsmith, R. H.; Sinks, L. E.; Kelley, R. F.; Betzen, L. J.; Liu, W.; Weiss, E. A.; Ratner, M. A.; Wasielewski, M. R. *Proc. Natl. Acad. Sci. U. S. A.* **2005**, *102*, 3540.
(53) Luo, L.; Choi, S. H.; Frisbie, C. D. *Chem. Mater.* **2011**, *23*, 631.
(54) Segal, D.; Nitzan, A.; Davis, W. B.; Wasielewski, M. R.; Ratner, M. A. *J. Phys. Chem. B* **2000**, *104*, 3817.
(55) Taherinia, D.; Smith, C. E.; Ghosh, S.; Odoh, S. O.; Balhorn, L.; Gagliardi, L.; Cramer, C. J.; Frisbie, C. D. *ACS Nano* **2016**, *10*, 4372.
(56) *Charge and Exciton Transport through Molecular Wires*; Siebbeles, L. D., Grozeman, F. C., Eds.; John Wiley & Sons, 2011.
(57) Marcus, R. A. *J. Chem. Phys.* **1965**, *43*, 679.
(58) Wang, D.; Fracasso, D.; Nurbawono, A.; Annadata, H. V.; Sangeeth, C. S. S.; Yuan, L.; Nijhuis, C. A. *Adv. Mater.* **2015**, *27*, 6689.
(59) *Impedance Spectroscopy: Theory, Experiment, and Applications*; Barsoukvo, E., Macdonald, J. R., Eds.; John Wiley & Sons, 2005.
(60) Landau, A.; Kronik, L.; Nitzan, A. *J. Comput. Theor. Nanosci.* **2008**, *5*, 535.
(61) Simeone, F. C.; Yoon, H. J.; Thuo, M. M.; Barber, J. R.; Smith, B.; Whitesides, G. M. *J. Am. Chem. Soc.* **2013**, *135*, 18131.
(62) Holm, R. *Electric Contacts: Theory and Application*; Springer: Berlin, Heidelberg, 1999; Vol. *1*.
(63) Beebe, J. M.; Engelkes, V. B.; Miller, L. L.; Frisbie, C. D. *J. Am. Chem. Soc.* **2002**, *124*, 11268.
(64) Engelkes, V. B.; Beebe, J. M.; Frisbie, C. D. *J. Am. Chem. Soc.* **2004**, *126*, 14287.
(65) Kim, B.; Beebe, J. M.; Jun, Y.; Zhu, X. Y.; Frisbie, G. D. *J. Am. Chem. Soc.* **2006**, *128*, 4970.
(66) Huang, M.-J.; Hsu, L.-Y.; Fu, M.-D.; Chuang, S.-T.; Tien, F.-W.; Chen, C.-H. *J. Am. Chem. Soc.* **2014**, *136*, 1832.
(67) Kim, T.; Liu, Z.-F.; Lee, C.; Neaton, J. B.; Venkataraman, L. *Proc. Natl. Acad. Sci. U. S. A.* **2014**, *111*, 10928.
(68) Castañeda Ocampo, O. E.; Gordiichuk, P.; Catarci, S.; Gautier, D. A.; Herrmann, A.; Chiechi, R. C. *J. Am. Chem. Soc.* **2015**, *137*, 8419.
(69) Cademartiri, L.; Thuo, M. M.; Nijhuis, C. A.; Reus, W. F.; Tricard, S.; Barber, J. R.; Sodhi, R. N. S.; Brodersen, P.; Kim, C.; Chiechi, R. C.; Whitesides, G. M. *J. Phys. Chem. C* **2012**, *116*, 10848.

DOI: 10.1021/jacs.6b02039
J. Am. Chem. Soc. 2016, 138, 7305−7314